Surface defect analysis on formed chalcogenide glass $Ge_{22}Se_{58}As_{20}$ lenses after the molding process

TIANFENG ZHOU,[1,*] QIN ZHOU,[1] JIAQING XIE,[1] XIAOHUA LIU,[1] XIBIN WANG,[1] HAIHUI RUAN [2,†]

[1]*Key Laboratory of Fundamental Science for Advanced Machining, Beijing Institute of Technology, Beijing 100081, China*
[2]*Department of Mechanical Engineering, The Hong Kong Polytechnic University, Hung Hom, Kowloon, Hong Kong*
**Corresponding author: zhoutf@bit.edu.cn*
[†]Corresponding author: haihui.ruan@polyu.edu.hk

Chalcogenide glass (ChG) is increasingly used in infrared optical systems owing to its excellent infrared optical properties and scalable production using precision glass molding (PGM). However, surface scratches affected by the molding temperature and microdimples on the lens surface caused by gas release seriously impair the quality of the formed lens. To reduce these surface defects when molding $Ge_{22}Se_{58}As_{20}$ ChG, the temperature effect must be studied, and the gas generation must be minimized, while the gas escape must be maximized. In this work, we studied the effect of temperature on the surface defects. Additionally, we studied the influences of the roughness and curvature of the contact surfaces as well as the pressing force on the formation of the microdimples. It was found that the molding temperature should be approximately 30°C higher than the softening temperature (T_s) to avoid surface scratches, the gas generation could be inhibited by increasing the pressing force and decreasing the roughness of the mold surface, and increasing the curvature difference between the mold and glass preform surfaces improved the gas escape.

OCIS codes: *(160.2750) Glass and other amorphous materials; (220.4610) Optical fabrication; (240.5770) Roughness; (240.6700) Surfaces.*

1. Introduction

Chalcogenide glass (ChG) has been extensively applied in infrared optical systems, such as in thermal imaging and night vision[1,2] owing to its wide transmission wave band from near to far infrared wavelengths and its excellent athermalization and achromatism properties[3]. To date, ChG lenses have mainly been machined using single-point diamond turning and ultraprecision grinding[4], by which subwavelength form accuracy and nanoscale surface roughness can be achieved. However, these methods are high cost with low efficiency. Precision glass molding (PGM) is usually used to produce oxide glass lenses in mass production to achieve high efficiency, which has been extended to molding ChG lenses[5,6] by a few researchers. In contrast to oxide glass, the optimum molding temperature of most ChGs is uncertain, and most ChGs have a greater saturated vapor pressure, which enables the release of trace gases during the molding process. When these gases cannot escape, the lens shape and surface quality[7] are severely impaired. To obtain ultraprecision lenses, the optimum molding temperature must be found. Also, the gas release and gas escape must be controlled.

Molding experiments using ChG were first reported by Zhang *et al.* at the French company Umicore IR Glass S.A.[4]. They produced spherical and diffractive lenses using $Ge_{22}As_{20}Se_{58}$ and $Ge_{20}Sb_{15}Se_{65}$. The maximum shape errors of their molded spherical and diffractive lenses were approximately 0.3 μm and 2 μm, respectively. They proposed that the molding temperature should be higher than the softening temperature (T_s) to achieve sufficient fluidity for filling the volume between the molds. In the same year, Zhang *et al.,* at the University of Rennes 1[6], reported a similar result that the shape error of the molded $Ge_{22}As_{20}Se_{58}$ spherical lens was approximately 0.4 μm and proposed that the molding temperature should be above T_s. They compared the transmission between a molded and a mechanically polished disc of ChG and corroborated that the molding process would not deteriorate the excellent transmission of ChG. Cha *et al.*[8] studied the effect of temperature on the molding process of $Ge_{10}As_{40}Se_{50}$, and they suggested that the ChG should be heated to a temperature less than the glass transition point (T_g) in the initial heating stage and molded at a temperature higher than T_s to prevent breakage. They also evaluated the quality of molded lenses based on the replication quality of the surface of the mold using IR transmittance and X-ray diffraction patterns and concluded that molding temperatures above the T_s would not deteriorate the optical properties of ChG. Liu *et al.*[9] conducted PGM numerical simulations for $Ge_{33}As_{12}Se_{55}$ to investigate the variations in its thermomechanical properties. Li *et al.*[10] developed a localized rapid heating process utilizing a fused silica wafer coated with a thin graphene layer which was heated by a power source to heat only the surface of the ChG. They concluded that localized rapid heating process by using graphene coated fused silica wafer was characterized

and can be readily implemented in replication of micro scale ChGs. Zhou *et al.*[11] evaluated the stress relaxation behavior of As_2S_3 above its glass transition temperature and calculated its refractive index change during cooling. Finally, they provided reliable references for viscoelastic characterization of As_2S_3 glass, and confirmed that the refractive index drop is strictly dependent on the cooling rate logarithmically by using Tool-Narayanaswamy-Moynihan model and that the slower the cooling rate is, the less the refractive index drop will be.

In our earlier studies, the Maxwell and Burgers models for creep and stress relaxation behavior have been used in finite element simulations of the glass molding process[12,13], and the deformation behavior of oxide glass at temperatures near the T_s has been modeled[14]. Based on these theoretical works, aspheric lenses [15,16], microgroove arrays and micropyramid arrays [17,18] have been successfully molded. To improve the flowability and reduce adhesion at high temperatures, ultrasonic-vibration-assisted molding has been used, which achieves better forming accuracy and surface quality[19,20], especially when fabricating microfeatures. However, the knowledge established on molding oxide glass cannot be directly applied to ChG because the uncertain molding temperatures and gas release during ChG molding, which can result in surface scratches and surface dimples as well as shape deviations, have not been considered. To achieve a clear understanding and to better control the molding quality, this work focuses on experimentally determining the effects of several processing parameters, such as the temperature, pressure, surface roughness and curvature difference, on the surface defects.

2. Glass molding experiments and surface defects

A. Cylindrical molding experiment using ChG

In A PGM process has four stages: heating, pressing, annealing and cooling, as schematically shown in Fig. 1. The cylindrical molding experiments were carried out by using an ultraprecision glass molding machine PFLF7 (SYS Co., Ltd., Japan) with seven stations, which are driven by seven cylinders. The cylindrical glass preforms were compressed between a pair of tungsten carbide molds with an inner sleeve to guide the motion of the upper mold and an outer sleeve to locate the lower mold. First, the heating stage is carried out at the stations 1, 2 and 3. Then the pressing is implemented at the station 4, where the force is fully applied to the upper mold until it is in place and then the force is shared by the outer sleeve. And annealing stages is implemented at the stations 4, 5 and 6 with reduced order constant force after the upper mold is in place. Finally, the cooling stage is applied at the station 7. The temperature, force and upper mold's travel during a PGM process are shown in Fig. 2. Nitrogen gas was purged into the molding chamber to exhaust the air, and the oxygen concentration in the forming chamber was below 10 ppm. The molds and the glasses were heated to the molding temperature using resistance rods that were inserted into the mold holders. The temperature of each mold holder was monitored and controlled with an accuracy of ±1°C. The lower mold remained stationary, while the upper mold was pressed by a pneumatic system, in which the pressure of the pneumatic actuator was regulated by an air compressor with an accuracy of ±0.01 MPa. The pressing force could be calculated knowing that the piston diameter was 76 mm.

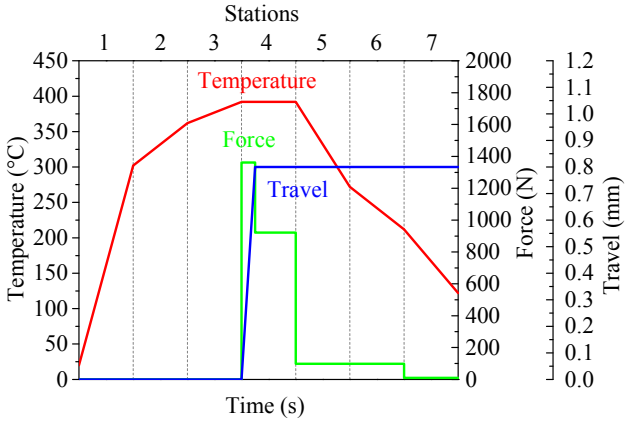

Fig. 2. The changes of temperature, force and upper mold's travel during a PGM process.

In this work, ChG $Ge_{22}Se_{58}As_{20}$ preforms (NHG Co., Ltd., China) with a height of 2.8 mm and a diameter of 7.8 mm were used. Their thermal and mechanical properties are listed in Table 1, which were provided by the glass maker NHG Co., Ltd. The data shown in Table 1 are nearly identical to Le Bourhis's[21] and Zhang's[4] results.

Table 1. Thermomechanical properties of GhG $Ge_{22}Se_{58}As_{20}$

Property	Value
Density ρ (g/cm^3)	4.41
Young's modulus E (GPa)	18.2
Poisson's ratio (ν)	0.28
Transition temperature T_g (°C)	282
Softening temperature T_s (°C)	352
Specific heat (J/(g·K))	0.36
Thermal expansion coefficient (10^{-6}/K)	17

B. Surface defects on the formed chalcogenide glass lens

The cylindrical molding experiments were conducted using molding temperatures ranging from 352°C to 392°C under a pressing force of 1362 N to find the suitable molding temperature. The ChG pillars formed at different molding temperatures are shown in Fig. 3 with the thickness of 2 mm. The glass broke when the molding temperature reached 352°C, and the surfaces became scratched at 362°C and 372°C. At the temperatures of 382°C and 392°C, fractures and scratches were not observed but many microdimples were, as shown in Fig. 4. The same observations were made using confocal laser scanning microscopy (CLSM). The scratch-like surface defects were actually caused be coalesced dimples. The maximum peak-to-valley height difference was 1.562 μm, which is within the infrared transmission waveband of $Ge_{22}Se_{58}As_{20}$ and reduced the infrared transmittance. To guarantee infrared transmittance, microdimples must be suppressed.

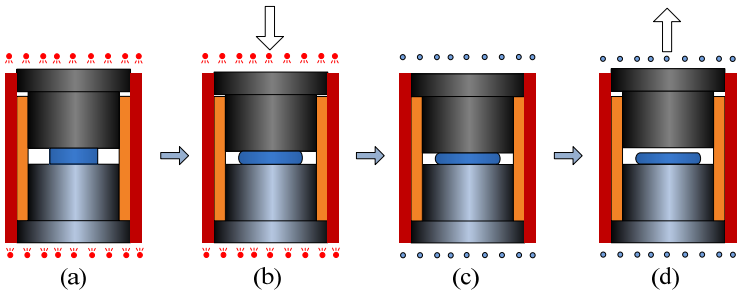

Fig. 1. Schematic diagram of four stages of a PGM cycle: (a) heating, (b) pressing, (c) annealing, and (d) cooling.

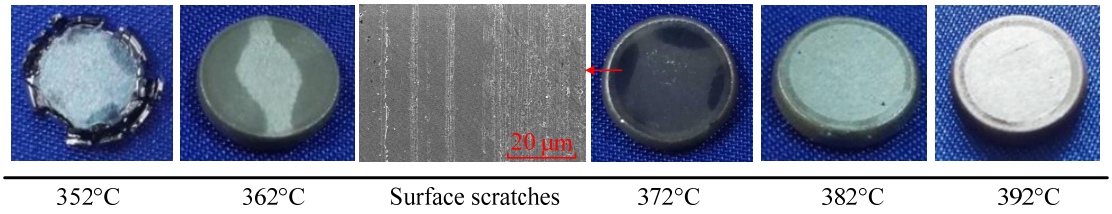

Fig. 3. The pillars formed at the molding temperatures between 352°C and 392°C under a pressing force of 1362 N.

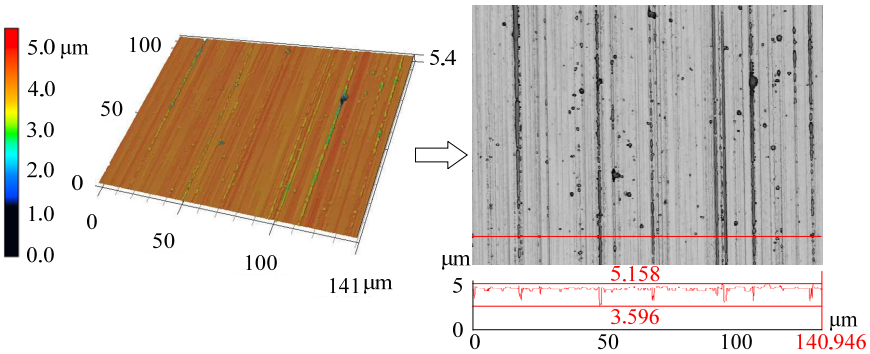

Fig. 4. The surface morphology and contour of a formed pillar at the molding temperature of 382°C.

As Zhang *et al.* at the French company Umicore IR Glass S.A.[4] indicated "defects in the glass such as bubbles" in their description of the glass production procedure and Niciu et al.[5] stated that higher temperature could lead to the evaporation of some sulphur in a violent way, microdimples were found on the surface of the formed pillar, which were presumably caused by the evaporation of selenide gas at high temperatures, which forms bubbles with various sizes. In addition, the chalcogen elements of ChG are easily affected by impurities during the preparation process and react with ions such as C^{+}, H^{+}, OH^{-} and O^{2-} [22-23]. To study the changes in the material after molding, we evaluated the change in the composition along the depth of the pillar before and after forming at 382°C using energy dispersive spectrometry (EDS), as shown in Fig. 5(a) and (b), respectively. For the preform, the atomic percentages were uniform and almost identical to the nominal composition. After molding, the atomic composition of Se was significantly reduced near the surface, indicating that Se was the dominant reactant for generating selenide gases.

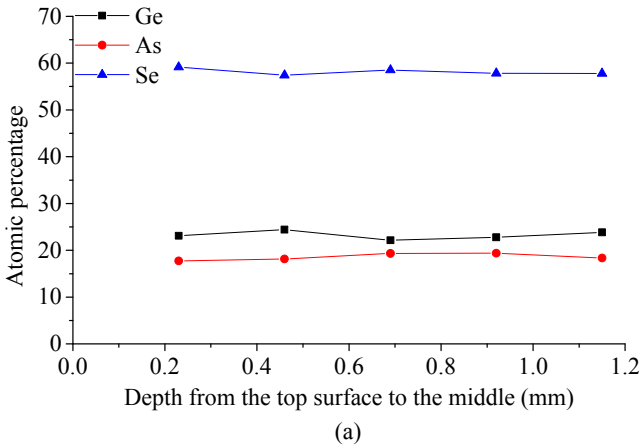

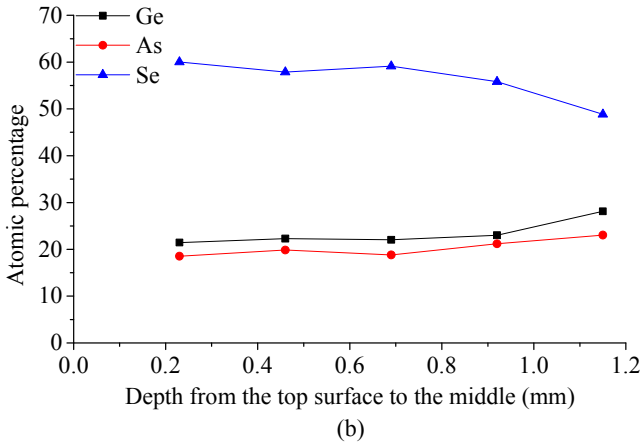

Fig. 5. Atomic percentage changes within the (a) glass preform and (b) formed pillar.

3. Analysis of the surface defects

A. Temperature effect on the surface defects

To study the temperature effect on the surface defects and to analyze the stress/strain distribution inside the glass, finite element method (FEM) simulations were performed using a commercial nonlinear FEM software, ABAQUS/Explicit. This software can be used to visualize the glass molding process and record the strain/stress distributions, internal temperature variations, and so on. A quarter model was established in order to reduce the computation time, and the assembly diagram is shown in Fig. 6. The thermomechanical properties of the ChG material are listed in Table 1, and the molds are described using the thermomechanical properties of tungsten carbide. Four analysis steps were used with the lower mold fixed: step-1 is to heat the molds and ChG to the molding temperature from the initial field temperature of 25°C, step-2 is to press the glass with a constant pressing force applied on the upper mold, step-3 is to set the temperature-displacement field coupling to hold the upper mold without a pressing force to simulate the stress relaxation process, and step-4 is to set the temperature-displacement field coupling to simulate annealing and cooling with the same conditions as those of the molding experiment. The contact between the mold and glass preform is set to surface-to-surface contact. The grid properties are set as an 8-node thermally coupled brick, while trilinear displacement and temperature, reduced integration and hourglass control are selected.

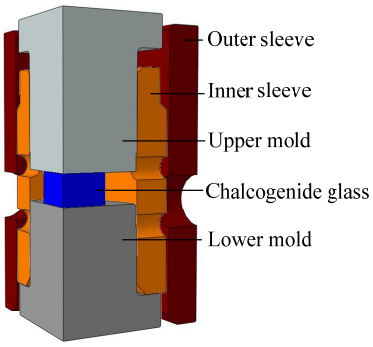

Fig. 6. Assembly diagram of the FEM simulation model.

The comparison between the experimental and simulated time-displacement curves is shown in Fig. 7. Overall, the simulated results agree well with experimental results, which verifies the credibility of the simulation. The temperature transferred from the mold to the glass with a temperature gradient, as shown in Fig. 8, achieving a layered distribution of temperatures along the axial direction. The surface of the glass reached molding temperature earlier than the middle of the glass. Fig. 9 shows the temperature increase curve of the ChG glass. The temperature began to increase quickly and then became level when approaching the target temperature value.

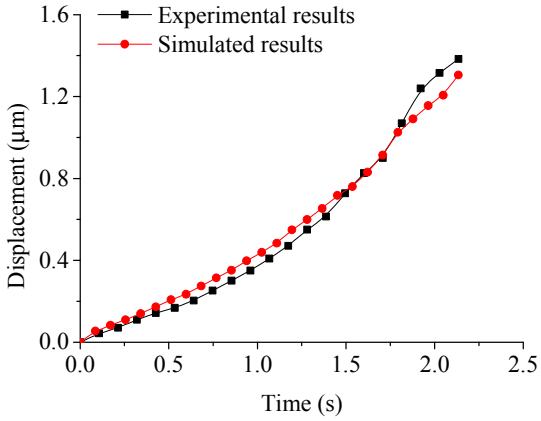

Fig. 7. Plots of the time-displacement curves of the experimental and simulated results under a pressing force of 1362 N at the molding temperature of 382°C.

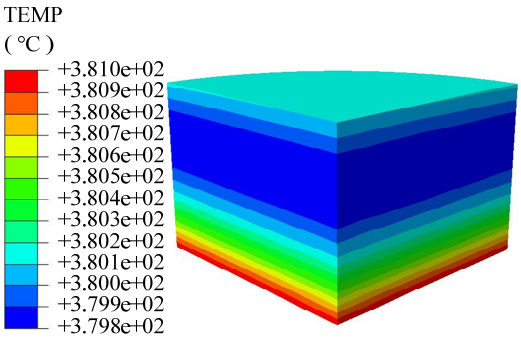

Fig. 8. Simulated results of the temperature conduction from the mold to the glass.

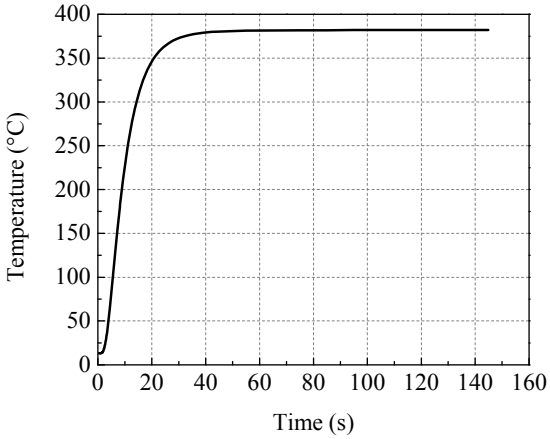

Fig. 9. Temperature increase curve over time for the ChG glass.

To study the ChG glass deformation at different molding temperatures, four kinds of axial temperature distributions were selected for compression and simulation, as shown in Fig. 10. Comparisons of the stress and strain distributions from the simulations of the four cases with the same downward displacement 0.63 mm are shown in Fig. 11(a) and (b). It can be seen that the axial stress distribution trends exhibit nearly the same parabola in all four cases, in which the stress in the middle is the largest. The axial strain distribution trend is also parabolic when the temperature is uniform and above T_s. However, the axial strain distribution trends change when the temperature is uneven. As shown in Fig. 11(b), the strain increases with the increase in the temperature, but strain is not present when the temperature is below 314°C. Therefore, breakage occurred due to the uneven strain when the temperature was T_g~T_s. Fig. 12(a) shows the simulated result of the strain distribution at uneven temperatures above T_s under a pressing force of 1362 N, and the deformation near the bottom is larger than in other places, which is consistent with the experimental result shown in Fig. 12(b). The simulations results indicate that the maximum diameter moved downward because of the larger strain near bottom.

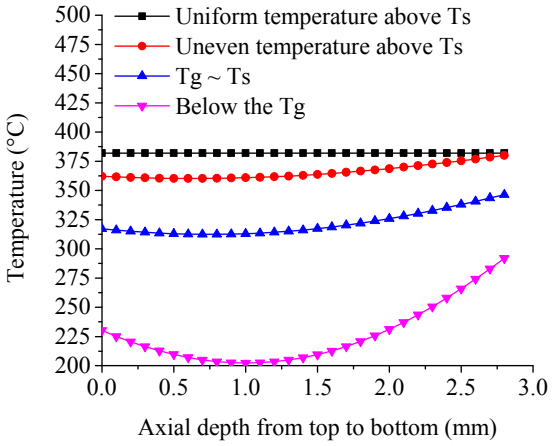

Fig. 10. Four kinds of axial temperature distributions.

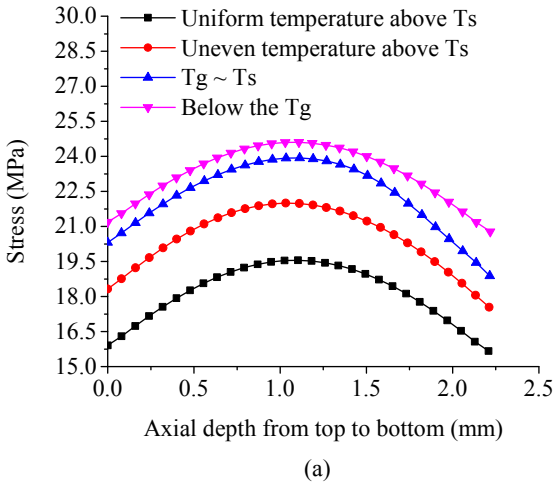

(a)

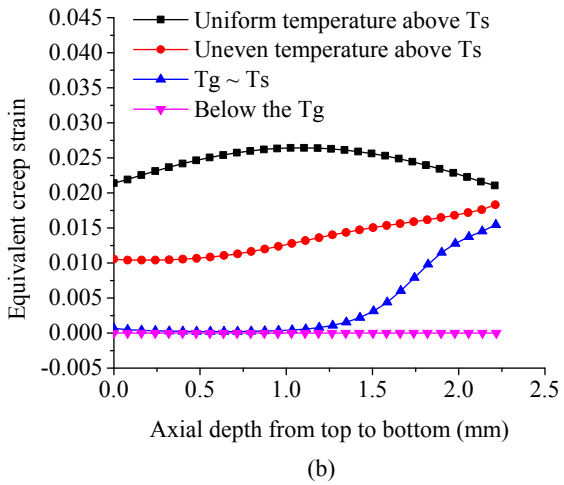

(b)

Fig. 11. Axial stress and strain distributions in the four cases with the same downward displacement of 0.63 mm under a pressing force of 1362 N.

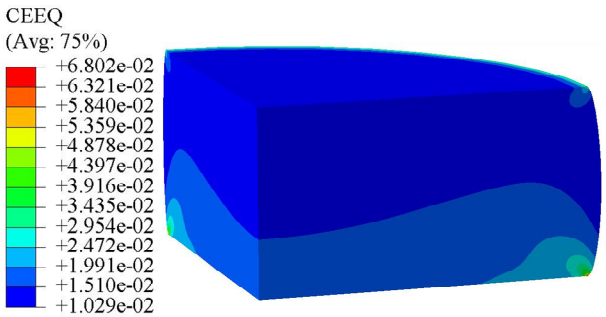

(a)

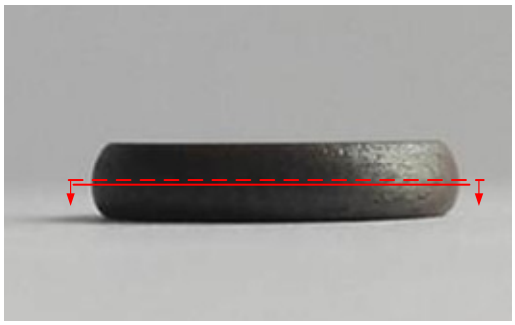

(b)

Fig. 12. Simulated and experimental results at uneven temperatures above T_s with the same downward displacement under a pressing force of 1362 N: (a) equivalent creep strain (CEEQ) distribution and (b) a formed pillar.

To analyze the formation of surface scratches, the stress and strain distributions on the top surface at different temperatures with the same downward displacement were studied under a pressing force of 1362 N. As shown in Fig. 13(a), the radial stress distribution trends are nearly the same at the four temperatures, in which the maximum stress is located near the edge. Meanwhile, the maximum strain is also located near the edge, as shown in Fig. 13(b), but the strain difference at the temperature of 362°C is much less than that at the temperature of 382°C, which explains that the cause of the surface scratches was insufficient strain near the edge of the glass pillar, as shown in Fig. 3.

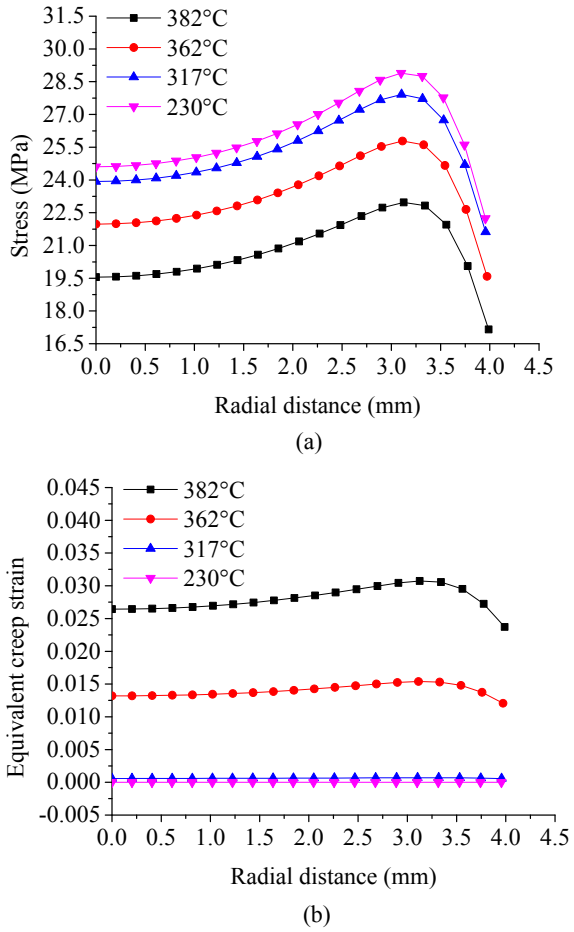

Fig. 13. Radial stress and strain distributions at the four temperatures with the same downward displacement under the pressing force of 1362 N.

B. Reduction mechanism of the microdimples

1. Temperature and pressure effects on the gas generation

To reduce the microdimples, gas generation should be reduced, and gas escape should be improved. For gas generation, the solubility of gas has been studied, and it can be expressed using A. Sieverts' square root law[24]:

$$S = k\sqrt{P}e^{-\Delta H/(RT)}. \quad (1)$$

where S is the dissolved concentration, k is a constant, P is the gas partial pressure, ΔH is the dissolution heat, R is the gas constant and T is temperature. The movements of the molecules become more intense as the temperature increases, leading to more reactions, smaller gas solubility and more gas generation. Pressure is another contributor that affects the gas solubility, besides the temperature. The gas density is greater with the increasing pressure, so the free molecular motion decreases, and the gas increasingly dissolves, as expressed by Eq. (1). According to Dalton's law of partial pressure, the total pressure is equal to the sum of the partial pressures of the mixed gas [25]. Meanwhile, based on Newton's third law[26], the total pressure increases with the increase in the pressing force. This law indicates that the gas solubility increases with the increase in the pressing force.

To quantify the effect of the temperature, the area ratios of the microdimples were evaluated. Five measuring spots, each of 63 × 44 μm, are equidistantly chosen in the direction of diameter on the upper surface of a formed pillar. And one spot locates at the center. The average area ratio is obtained these five surface micrographs. More surface micrograph can be used in calculating the average area ratio, but the results are almost identical. In order to make the results more vivid, the surface micrographs at the center are shown in Fig. 14 and 15, which have indicated the great difference. The area ratio of the latter is also measured by this method. The area ratios of the microdimple areas increased almost logarithmically with the molding temperature, as shown in Fig. 14. By extrapolating the trend line in Fig. 14, we could estimate that the temperature for preventing microdimple was approximately 379.8°C. However, this temperature is too low and could lead to surface scratching. In our experiment, surface scratches remained even after molding at 380°C. Therefore, it was inferred that the optimum temperature would be between 380 and 382°C. In the subsequent study, we fixed the molding temperature to be 382°C and focused on other parameters that could minimize the effects of gas release when gas release was inevitable.

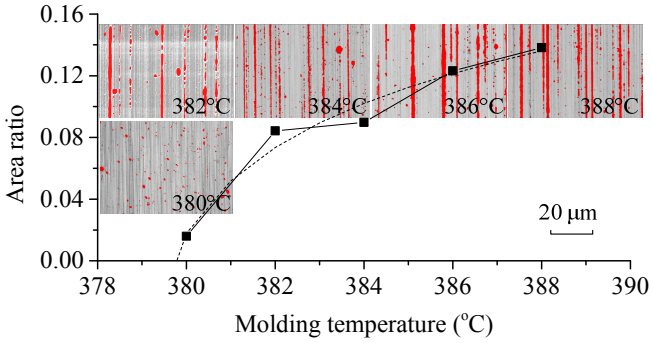

Fig. 14. Area ratios of the microdimples at different molding temperatures under a pressing force of 1362 N.

Meanwhile, the area ratios of the microdimples with different pressing forces were also evaluated. As shown in Fig. 15, the area ratios of the microdimples decrease with the increase in the pressing force at a molding temperature of 382°C. They decrease slowly from 1362 N to 2723 N and then decrease rapidly from 2723 N to 4085 N. Therefore, it can be assumed that if the contact pressure is larger than the saturated vapor pressure of the ChG, the gas will no longer be generated.

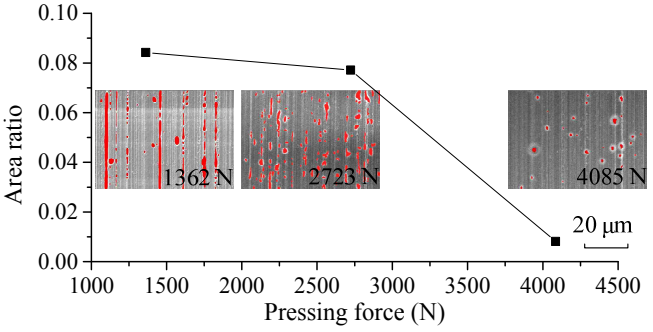

Fig. 15. Area ratios of the microdimples of the formed pillars under different pressing forces at the molding temperature of 382°C.

2. Contact surface roughness effect on the microdimples

To decrease the occurrence of microdimples on the glass surface, the effect of the contact surface roughness was studied. Due to the surface microstructures of the mold and glass, the enclosed spaces resulted in a lower local pressure, as shown in Fig. 16. The pressure of the enclosed spaces was lower than the saturated vapor pressure of

ChG, which intensified the evaporation of selenide gases and led to the morphology that exhibited incomplete reproduction and microdimples. However, the pressure of the joined surfaces was much higher than the saturated vapor pressure of ChG, and hence, these surfaces were reproduced in full. When the contact surfaces were smoother, the number of enclosed spaces was lower, and the gas generation decreased. In contrast, the enclosed spaces resulted in enclosed gas, which impeded gas escape. When the contact surfaces were smoother, the gas escaped more completely, as shown in Fig. 17, which also led to a better surface quality.

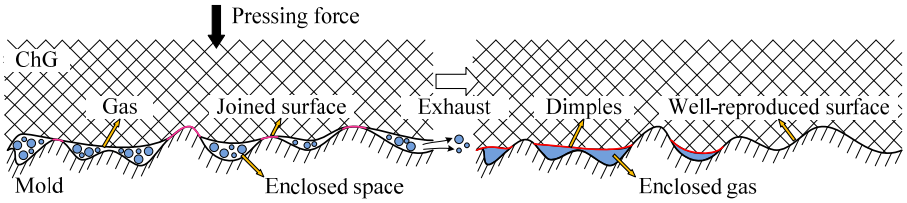

Fig. 16. Schematic diagram of the microdimple formation in during the glass molding process.

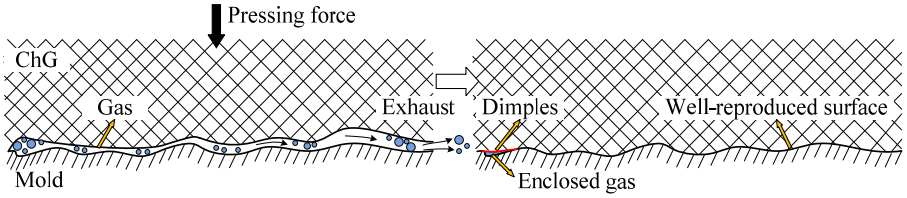

Fig. 17. Schematic diagram of the microdimple formation during the glass molding process with a high precision mold.

To verify the contact surface roughness effect, three groups of molds were prepared with surface roughness (Ra) values of 7 nm, 62 nm and 835 nm, respectively. The surface roughness (Ra) of the glass preform was 10 nm. The glass molding experiments were carried out under the pressing force of 4085 N at the molding temperature of 382°C. Fig. 18 shows the area ratios of the microdimples under different mold surface roughness values. It can be concluded that smoother mold surfaces led to fewer microdimples, which verified the notion of the effect of the contact surface roughness, as shown in Figs. 16 and 17. When the mold surface roughness (Ra) was 7 nm, the area ratio of the microdimples reached its minimum value. Moreover, 7 nm meets the precision requirement of infrared optical applications, so it was chosen for the next study.

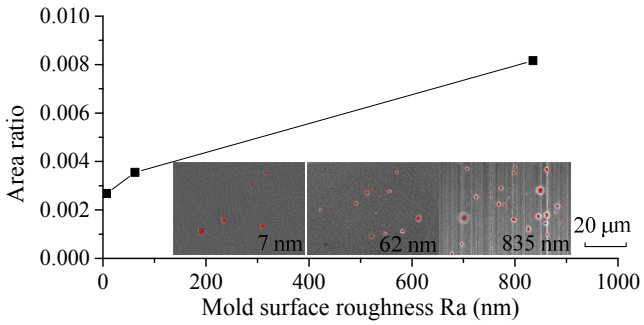

Fig. 18. Area ratios of the microdimples of the formed pillars with different mold surface roughness values under the pressure force of 4085 N at the molding temperature of 382°C.

3. Contact surface curvature effects on the microdimples

The effect of the surface curvature of the glass preforms was also studied. The mold surfaces were planar with a roughness (Ra) of 7 nm. The glass preforms had spherical surfaces with different curvature radii. It is impracticable to control a uniform pressure between contact surfaces. Therefore, in our experimental study of the effect of surface curvature, we can only guarantee external force to be the same. The effect of curvature is mixed with the pressure effect since the smaller radius of the glass surface brings about the smaller contact area and the larger contact pressure, which can reduce microdimples. In addition, when the glass surface is more curved, the gas escape becomes easier as shown in Fig. 19. This latter effect is different from the effect of pressure and is the main point of our discussion in this section. It can be seen from Fig. 20 that the area ratios of the microdimples of the formed pillars decreased, or were even completely eliminated, with the decrease in the glass curvature radius. The surface roughness (Ra) of a formed pillar without microdimple can reach 20 nm.

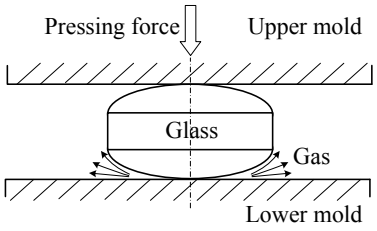

Fig. 19 Gas escape mode during the spherical glass molding process.

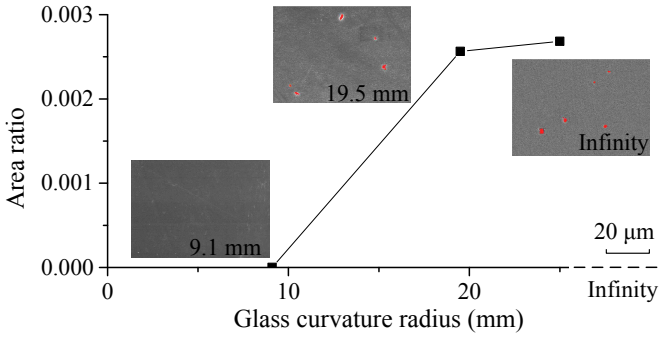

Fig. 20 Area ratios of the microdimples of the formed lenses with different glass surface curvature radii under 4085 N with a molding temperature of 382°C.

Another experimental scheme to study the contact surface curvature effect included reducing the curvature radius of the mold surface, as shown in Fig. 21 (a). The glass surface was plain with a roughness (Ra) of 10 nm. The upper mold had a spherical surface with a curvature radius of 2.5 mm. After the experiment, the formed pillar had a convex surface, a flat surface and a concave surface as shown in Fig. 21 (d), (e) and (f), respectively. Moreover, microdimples were not present on these surfaces, which means that the microdimples could be eliminated by reducing the curvature radius of the mold. It was also concluded that the gas generation and escape could be improved by enlarging the curvature difference between the glass surface and the mold surface, either by reducing the curvature radius of the glass or the molds.

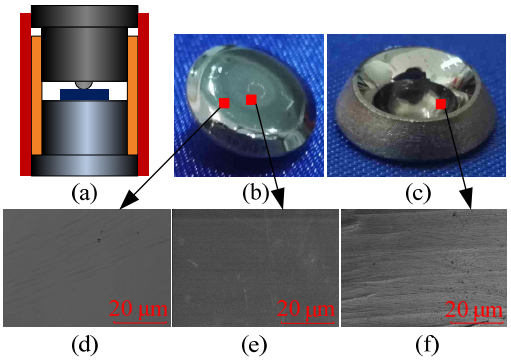

Fig. 21. Glass molding experiments with spherical molds: (a) experimental scheme, (b) the lower surface of a formed pillar, (c) the upper surface of a formed pillar, (d) the micromorphology of the convex surface, (e) the micromorphology of the flat surface and (f) the micromorphology of the concave surface.

4. Conclusions

To analyze the surface defects on chalcogenide glass (ChG) during the molding process, cylindrical molding experiments were carried out, and various molding temperatures were tested. The causes of the microdimples were analyzed, and the temperature effects on the stress and strain distribution were studied. To reduce the occurrence of microdimples, the processing parameters, including the temperature, pressure, surface roughness and curvature difference, were studied to decrease the gas generation and increase the gas escape. The main findings are summarized as follows:

(1) The molding temperature should be approximately 30°C higher than the softening temperature (T_s), and strain was not observed when the temperature was below 314°C. Brittle cracks and surface scratches may occur if the molding temperature is below 380°C. When the temperature is over 382°C, microdimples may occur due to gas generation and the inability of the gas to escape. The maximum diameter of the formed pillar moved from the middle layer during the application of uneven temperature.

(2) To decrease the gas generation, the pressing force should be sufficiently high to make the internal stress of ChG greater than the saturated vapor pressure. The contact surface between ChG and the molds should be sufficiently smooth to decrease the number of enclosed spaces and prevent lowering the local pressure.

(3) To increase the gas escape, the contact surface between the ChG and molds should be sufficiently smooth to decrease the number of enclosed spaces and reduce the volume of sealed gas. The difference in the curvature radius between the glass and the mold should be sufficiently large to facilitate gas escape.

Acknowledgment

This work has been supported by National Key Basic Research Program of China (No. 2015CB059900), National Natural Science Foundation of China (No. 51375050), the Early Career Scheme (ECS) of the Hong Kong Research Grants Council (Grant No. 25200515, Account No. F-PP27) and the Internal Research Funds (G-YBDH) of Hong Kong Polytechnic University. The authors would also like to thank the supporting from Fok Ying-Tong Education Foundation for Young Teachers in the Higher Education Institutions of China (No. 151052).

References

1. B. Tang, Y. Yang, Y.Y. Fan, L Zhang, "Barium gallogermanate glass ceramics for infrared applications," J. Mater. Sci. Technol. 26, 558-563 (2010).
2. B. Bureau, X.H. Zhang, F. Smektala, J.L. Adam, J. Troles, H.L. Ma, C. Boussard-Plèdel, J. Lucas, P. Lucas, D. Le Coq, M.R. Riley, J.H. Simmons, "Recent advances in chalcogenide glasses," J Non-Cryst Solids 345&346, 276-283 (2004).
3. C.W. Kuo, "Achromatic triplet and athermalized lens assembly for both midwave and longwave infrared spectra," Opt. Eng. 53, 1-7 (2014).
4. X.H. Zhang, Y. Guimond, Y.Bellec, "Production of complex chalcogenide glass optics by molding for thermal imaging," J. Non-cryst. Solids 326-327, 519-523 (2003).
5. H. Niciu, M. Popescu, A.Velea, A. Lorinczi, A. Manea, D. Niciu, M. Lazarescu, "Moulding procedure for the preparation of infrared glassy microlenses and prisms based on arsenic sulphide chalcogenide glass," Chalcogenide Lett. 7, 625-629 (2010).
6. X. Zhang, H. Ma, J. Lucas, "Applications of chalcogenide glass bulks and fibres," J. Optoelectron. Adv. M. 5, 1327-1333 (2003).
7. A.R. Hilton, *Chalcogenide Glasses for Infrared Optics*, New York: McGraw-Hill Companies, 2010.
8. D.H. Cha, H.J. Kim, H.S. Park, Y. Hwang, J.H. Kim, J.H. Hong, K.S. Lee, "Effect of temperature on the molding of chalcogenide glass lenses for infrared imaging applications," Appl. Optics 49, 1607-1613 (2010).
9. W.G. Liu, P. Shen, N. Jin, "Viscoelastic properties of chalcogenide glasses and the simulation of their molding processes," Phys. Procedia 19, 422-425 (2011).
10. H. Li, P. He, J. Yu, L.J. Lee, A.Y. Yi, "Localized rapid heating process for precision chalcogenide glass molding," Opt. Laser Eng. 73, 62-68 (2015).
11 J. Zhou, J.F. Yu, L.J. Lee, L.G. Shen, A.Y. Yi, "Stress relaxation and refractive index change of As_2S_3 in compression molding," Int. J. Appl. Glass Sci. DOI: 10.1111/ijag.12244 (2016).
12. T.F. Zhou, J.W. Yan, T. Kuriyagawa, "Evaluating the viscoelastic properties of glass above transition temperature for numerical modeling of lens molding process," in *International Symposium on Photoelectronic Detection and Imaging 2007*, L.W. Zhou ed. (Proc. of SPIE, 2008), p. 662403-1-11.
13. T.F. Zhou, J.W. Yan, J. Masuda, T. Kuriyagawa, "Investigation on The Viscoelasticity of Optical Glass in Ultraprecision Lens Molding Process," J. Mater. Process. Tech. 209, 4484-4489 (2009).
14. J.W. Yan, T.F. Zhou, J. Masuda, T. Kuriyagawa, "Modeling High-temperature Glass Molding Process by Coupling Heat Transfer and Viscous Deformation Analysis," Precis. Eng. 33, 150-159 (2009).
15. J.W. Yan, T.F. Zhou, N. Yoshihara, T. Kuriyagawa, "Shape Transferability and Microscopic Deformation of Mold Dies in Aspherical Glass Lens Molding Press," J. Manuf. Tech. Res. 1, 85-102 (2009).

16. T.F. Zhou, J.W. Yan, N. Yoshihara, T. Kuriyagawa, “Study on Nonisothermal Glass Molding Press for Aspherical Lens,” J. Adv Mech Des Syst. 4, 806-815 (2010).
17. T.F. Zhou, J.W. Yan, T. Kuriyagawa, “Comparing Microgroove Array Forming with Micropyramid Array Forming in the Glass Molding Press,” Key Eng. Mater. 447-448, 361-365 (2010).
18. T.F. Zhou, J.W. Yan, J. Masuda, T. Oowada, T. Kuriyagawa, “Investigation on Shape Transferability in Ultraprecision Glass Molding Press for Microgrooves,” Precis. Eng. 35, 214-220 (2011).
19. J.Q. Xie, T.F. Zhou, Y. Liu, T. Oowada, X.B. Wang, “Mechanism Study on Microgroove Forming by Ultrasonic Vibration Assisted Hot Pressing,” Precis. Eng. 46, 270-277 (2016).
20. T.F. Zhou, J.Q. Xie, J.W. Yan, K. Tsunemoto, X.B. Wang, “Improvement of glass formability in ultrasonic vibration assisted molding process,” Int. J. Precis. Eng. Man. 18, 57-62 (2017).
21. E. Le Bourhis, P. Gadaud, J.-P. Guin, N. Tournerie, X.H. Zhang, J. Lucas, T. Rouxel, “Temperature dependence of the mechanical behaviour of a GeAsSe glass,” Scripta Mater. 45, 317-323 (2001).
22. A. VAŠKO, D. LEŽAL, I. SRB, “Oxygen impurities and defects in chalcogenide glasses,” J Non-Cryst Solids 4, 311-321 (1970).
23. C.T. Moynihan, P.B. Macedo, M.S. Maklad, R.K. Mohr and R.E. Howard, “Intrinsic and impurity infrared absorption in As_2Se_3 glass,” J Non-Cryst Solids 17, 369-385 (1975).
24. C.K. Gupta, *Chemical metallurgy: principles and practice*, Wiley-VCH, 2003, p. 273.
25. M.S. Silberberg, *Chemistry: the molecular nature of matter and change (5th ed.)*, Boston: McGraw-Hill, 2009, p. 206.
26. J.D. Kelley, J.J. Leventhal, *Newtonian Physics// Problems in Classical and Quantum Mechanics*, Springer International Publishing, 2017.